American Mineralogist, Volume 69, pages 954–960, 1984

Diffraction study of annealing of metamict samarskite

LUDWIG KELLER[1]

Department of Materials Science and Engineering
School of Engineering and Applied Science
University of California, Los Angeles
Los Angeles, California 90024

Abstract

X-ray diffraction of metamict samarskite, heated in air for 15 min above its crystallization temperature of 870°C, indicates that its premetamict structure is not restored. Instead, the heating results in the formation of three stoichiometric phases which are (Y,RE)(Nb,Ta)O_4, $FeNbO_4$ and $U_3O_8 \cdot 1.5Nb_2O_5$. Broadening of X-ray line profiles of the crystalline reaction products is analyzed as stress broadening caused by new phase nuclei. It is assumed that during heating nonuniform strains are produced by small precipitates (10–100Å) of intermediate phases which press against growing crystallites of the stable reaction products. For the $FeNbO_4$ phase the concentration of stress causing nuclei is estimated to be 5 vol.% at 870°C and 1 vol.% at 1240°C. No line broadening is observed at 1470°C which indicates that stresses are relaxed and the precipitates are dissolved at that temperature. Volume differences between matrix and final crystallization products cause the compact material to disintegrate into loose powder during heating. Crystalline domains in residual metamict material are detected by electron diffraction. Because of their low concentration (<1%), these domains cannot be considered typical of the metamict state of samarskite. From the annealing behavior it is concluded that crystallization of metamict samarskite is dominated by nucleation processes which cause microcracking several hundred °C below crystallization temperature.

Introduction

Minerals occurring in the metamict state are commonly understood to have lost their crystalline structure through a process called metamictization. X-ray diffraction is an important method for investigating the metamict state, with a few broad, diffuse diffraction maxima (halos) observed rather than sharp Bragg peaks. Entirely crystalline phases can usually be obtained by sufficient heating of metamict minerals (Berman, 1955; Lima de Faria, 1964), but it is well known that the structures obtained are not necessarily the same as those of the premetamict state (Ewing and Ehlmann, 1975a).

This study focusses on the crystallization behavior of samarskite and its implications on defining the metamict state. The term "metamict" was introduced by Broegger (1893) as indicative of the unique properties of minerals with a high content of rare earth elements (samarskite, fergusonite, yttrotantalite, euxenite, gadolinite etc.): they become amorphous from an orginally crystalline state without loosing their plane bounding faces and show optical isotropy and a decrease in density. Since then many more minerals, including simple oxides, silicates, titanates and phosphates, have been identified as metamict. It is generally agreed upon now that the metamict state results from nuclear radiation of radioactive elements contained with these minerals. Responses to internal radiation, however, vary from mineral to mineral, even if they only differ in their modification (Cartz et al., 1981). So far, no definite conclusions have been reached about this phenomenon.

Experimental procedure

All heatings were carried out in air in a SiC-tube furnace. The material (Mitchell County, N.C.), in compact form, was contained in a Pt-boat. The working temperatures of 870, 1050, 1240 and 1470±10°C were reached within 15 min by rampheating, held for 15 min, and then cooled by shutting off the furnace. The first temperature of 870°C was chosen because differential thermal analysis in air showed a strong exothermic peak at 865°C accompanied by a glowing or "pyrognomic

[1] Present address: Tokamak Fusion Laboratory, School of Engineering and Applied Science, University of California, Los Angeles, Los Angeles, California 90024.

0003–004X/84/0910–0954$02.00

effect'' which is observed on many metamict minerals when they start to crystallize. For samples heated to a maximum temperature <865°C, no crystalline structure could be detected by diffraction.

Line broadening experiments require a high resolution diffraction apparatus. A HUBER Guinier powder diffraction system, consisting of a focussing quartz monochromator (Johannsen type) combined with a Seemann-Bohlin chamber, was used, at room temperature. The diffraction patterns were recorded on single layer X-ray film to maintain the strict focussing requirements. For optimal line resolution, an AEG-TELEFUNKEN X-ray tube with a Cu-target and an optical focal line width of 5 μm was used. The resultant fluorescent radiation from iron in the sample had a negligible effect on the broadening study. The system resolution was calibrated with a $CaWO_4$ (scheelite) powder standard, as recommended by the manufacturer. Powders were prepared by crushing material in a stainless steel mortar with a single smash and collecting the dust (−325 mesh size). Thus grinding and possible crystallization effects were avoided. Guinier powder diffraction was also used for phase analysis. The *hkl*-indexing and lattice parameter refinement were done with the computer method of Evans et al. (1963).

To analyze any crystalline regions present in the untreated metamict material which may be too small in size and concentration to be detected by XRD, electron powder diffraction and selected area diffraction (SAD) were carried out in a SIEMENS ELMISKOP 1A. For 50–100 keV electrons and a mineral density of about 6 g/cm^3 the maximum thickness for transmission was estimated as 1000 to 3000Å. By successive sedimentation in destilled water and specially designed glass containers (Atterberg cylinders) enough particles <1 μm were obtained for analysis. A few hundred grams of −325 mesh size powder, as prepared in this way, was necessary to start the separation process. It was expected that at least a fraction of the particles would be thin enough to be penetrated by electrons. The TEM sample carriers were 20 μm hole size Cu-grids covered with a film of collodion, reinforced by a carbon coating. The collected particles were suspended in alcohol and sprayed onto the grids to obtain a homogenous distribution. The camera length for both powder diffraction (only condenser lenses modulated the e-beam) and SAD were determined and calibrated with a TlCl standard (Witt, 1964).

Line profile analysis

Profiles of the diffraction lines were evaluated with an automated stepping, double beam densitometer (JOYCE LOEBL). Both stepping width and a horizontal slit width were chosen as 15 μm to compensate for step resolution and film grain size. To separate the ''physical broadening'' of interest from ''instrumental broadening'' in the line profiles, profiles were expressed as Fourier series and were numerically deconvoluted by Stokes (1949) method. A computer code was written to carry out the Fourier transforms. The profiles of instrumental broadening were obtained from diffraction lines of a $CaWO_4$ standard, since fine grain size powder of $CaWO_4$ is considered to be strain-free and does not produce a crystallite size broadening effect. Each pair—observed profile and $CaWO_4$ reference profile—were measured at approximately the same diffraction angle since instrumental broadening is 2Θ dependent. Overlapping lines were separated and drawn out to their tails by hand, assuming symmetric profiles. Stokes method of line separation works well only if the reference line is narrow compared to the observed line. At a ratio of integral widths of observed profile to reference profile smaller than 2, deconvolution yielded unreliable physical profiles distorted by superimposed oscillations which are an unavoidable consequence of truncation errors in the Fourier analysis. In this case (at low diffraction angles and the highest temperature (1240°C) the observed and reference profiles were numerically fitted by least squares method to Cauchy functions which exhibit the simple relationships:

$$\mathrm{IHW} = \left[\int_{-\infty}^{+\infty} dx/(1 + a^2x^2)\right] \Big/ y_{max} = \pi/a$$

where y is normalized to 1, and

$$\mathrm{IHW} = \mathrm{IHW_m} + \mathrm{IHW_n}$$

$\mathrm{IHW_m}$ and $\mathrm{IHW_n}$ are the integral widths of two Cauchy profiles m and n. The values of IHW obtained by this method are less accurate than those from deconvolution but are still within the error of measurement.

XRD theory distinguishes between two broadening effects for a powder diffraction line: the crystallite size broadening effect and the broadening effect caused by lattice distortion (e.g., strain) on an atomic scale. The angular dependences are respectively:

$$\mathrm{IHW_{cryst}} = \lambda/L \cos\Theta$$

and

$$\mathrm{IHW_{dist}} = C \tan\Theta$$

where λ is wavelength, L crystallite size, Θ diffraction angle and C distortion parameter. $\mathrm{IHW_{cryst}}$, the width of a crystallite size broadened line, is a sensitive function of up to moderate diffraction angles ($\pi/4$) whereas $\mathrm{IHW_{dist}}$, the width of a lattice distortion broadened line, is not. If both effects contribute to the line broadening, the method of Warren and Averbach (1952) is the rigorous way to separate them. If only one effect dominates there is a much simpler way to ascertain this. Assuming Cauchy type profiles,

$$\mathrm{IHW_{obs}} - \mathrm{IHW_{ref}} = \mathrm{IHW_{cryst}} + \mathrm{IHW_{dist}}$$
$$= \lambda/L\cos\Theta + C\tan\Theta = \mathrm{IHW_{phys}}$$

and

$$[(\cos\Theta)/\lambda]\ IHW_{phys} = 1/L + C(\sin\Theta)/\lambda$$

In plots of $[(\cos\Theta)/\lambda]\ IHW_{phys}$ against $(\sin\Theta)/\lambda$, the slope of the linear fit yields C and the intercept of the ordinate is inversely proportional to the crystallite size. According to Guinier (1963) crystallite size broadening is observable up to 2000Å at best. Here, the noncubic, low symmetry crystal systems result in considerable deviations of L and C from linearity and average values are thus obtained by linear regression over many diffraction lines (*hkl*).

Results

Phase analysis

Up to 865°C no crystalline structure could be detected. The X-ray diffraction pattern consisted of a diffuse halo as reported and analyzed by Keller and Wagner (1982). Above 500°C the halo became sharper and, at 870°C, it split into two broad peaks. However, the peaks were too broad and overlapped too much for reliable phase identification. At 1050°C, the diffraction lines became sharper but the pattern did not vary much from that at 870°C. Line broadening disappeared at 1470°C. The diffraction lines of the reaction product at 1050°C matched, except for small differences in intensity, the *d*-values of recrystallized samarskite investigated but not indexed by Berman (1955) (JCPDS-Nr. 10-398). Komkov (1965a, b) recognized crystallized samarskite (from heating in air at 1050°C) as a three-phase mixture consisting of monoclinic (Y,RE) $(Nb,Ta)O_4$, orthorhombic $FeNbO_4$ and orthorhombic $U_3O_8 \cdot 1.5Nb_2O_5$. In Table 1, the observed d-values are allocated among the indexed reflections of the three phases. The lattice parameters of the three phases at 1050°C are given in Table 2. The $FeNbO_4$ phase is not observed at 1470°C; this orthorhombic phase is stable up to 1380°C (DTA showed an exothermal peak at 1385°C) and its melting point lies at 1475°C (Roth and Warning, 1964). The $U_3O_8 \cdot 1.5\ Nb_2O_5$ phase, less well documented, is not observed at 1470°C either. Besides the (Y,RE) $(Nb,Ta)O_4$ phase, at 1470°C a Y_2O_3 and a TaO_2 phase were observed plus unidentified lines, which probably belong to an iron-oxide.

Line broadening

The crystalline reaction products at 870, 1050 and 1240°C showed X-ray line broadening which decreased with increasing temperature. At 1470°C no physical broadening could be found. The character of broadening is determined both qualitatively and quantitatively. The qualitative test is demonstrated best with the $FeNbO_4$ phase; Figure 1 shows the test plot at 1050 and 1240°C, with the broadening at 1240°C about half that at 1050°C. The intercept value for crystallite size is far too high

Table 1. Indexed *d*-spacings of samarskite annealed at 1050°C in air

I/I_o	d_{obs} [Å]	Δd [Å]	(hkl) $(Y,RE)(Nb,Ta)O_4$	(hkl) $FeNbO_4$	(hkl) U_3O_8 $1.5Nb_2O_5$
45	4.04	0.02			(001)
25	3.59	0.01		(110)	
70	3.24	"			(200)
30	3.12	"	(121)		
20	3.06	"			
40	3.00	"	(130)		
20	2.96	"	(031)/(121)		
100	2.923	0.009		(111)	
10	2.813	"		(020)	
15	2.761	0.008	(040)		
10	2.65 b	"	(200)		
10	2.60 b	0.007			(111)
45	2.518	"	(002)	(002)	(201)
15	2.450	0.006		(021)	
10	2.336	"		(200)	
10	2.172	0.005	(141)/(122)	(121)	
10	2.055	0.004		(112)	
10	2.016	"	(051)		
10	1.921	"			(020)
15	1.91 b	"	(240)		
15	1.892	"	(132)		
20	1.868	"	(151)/(042)	(022)	
10	1.835	0.003			(120)
15	1.738	"		(130)	
25	1.708	"		(202)	
30	1.688	"		(221)	
10	1.63 vb	"	(321)		
15	1.57 vb	0.002			(212)
15	1.51 vb	"		(113)	
10	1.50 vb	"			
15	1.436	"		(331)/(025)	
10	1.428	"		(132)	

Line profile analysis not made for overlapping lines
b : broad
vb : very broad

Table 2. Refined lattice parameters of reaction products of annealed samarskite (1050°C in air)

$(Y,RE)(Nb,Ta)O_4$	$FeNbO_4$	U_3O_8 1.5Nb_2O_5
a = 5.31 ± 0.01 Å	a = 5.004 ± 0.004 Å	a = 6.46 ± 0.05 Å
b = 11.02 ± 0.02 Å	b = 5.620 ± 0.004 Å	b = 3.84 ± 0.02 Å
c = 5.03 ± 0.04 Å	c = 4.669 ± 0.004 Å	c = 4.07 ± 0.03 Å
β = 94 ± 0.7°		

(>2000Å) to cause size broadening. Least-squares fits yield approximately the same intercept, which indicates that small crystallite size has little effect on line broadening >1050°C. This allows a direct plot of IHW versus tanΘ from which the distortion parameter C can be deduced (Fig. 2). In Figure 3, IHW values of the $U_3O_8 \cdot 1.5Nb_2O_5$ phase are plotted for 1050 and 1240°C, again with a decrease to about half at the higher temperature. The $(Y,RE)(Nb,Ta)O_4$ phase could only be analyzed at 1240°C (see Fig. 4) since the profiles at 1050°C were too weak to be properly resolved from the background and at 1470°C no broadening could be detected. This phase, however, differs from the others in having a higher degree of distortion.

Model of "nuclei of a new phase"

The underlying theory and details of X-ray line broadening of crystals containing nuclei of a new phase are extensively treated by Krivoglaz (1969). Only the most important relationships are summarized here. Two stages of lattice distortions can be distinguished by X-ray scattering:

(1) Moderate distortions cause a weakening of the Bragg reflections (*hkl*)

$$I = I_0 \exp(-2M)$$

where M is the distortion parameter (not discussed here).

(2) severe distortions replace Bragg peaks with diffuse scattering maxima; the IHW of these Cauchy type distributions relate directly to lattice distortions as

$$IHW = C \tan\Theta.$$

Broadening can be caused by defects, or it may result by particles of a precipitating new phase, of the order of 10–100Å in size and differing in composition and/or structure from the matrix. During precipitation the nuclei create a static displacement around them:

$$\vec{u} = c\,\vec{r}_{ts}/r^3$$

$\vec{u}$ is the displacement vector which falls off on a Coulomb law and $\vec{r}_{ts}$ is a vector from the defect position t to the s-th cell of the nucleus. The distortion parameter is connected to a change of the unit cell parameters via the elastic properties of the solid. For elastically isotropic crystals,

$$IHW = 7.6\,\alpha\,cn\tan\Theta$$

with $\alpha=[(1+\sigma)\Delta V](9(1-\sigma)V)^{-1}$, where σ is the Poisson ratio of the material, V is the unit cell volume and cn, the distortion parameter, is the volume concentration of compression causing phase nuclei.

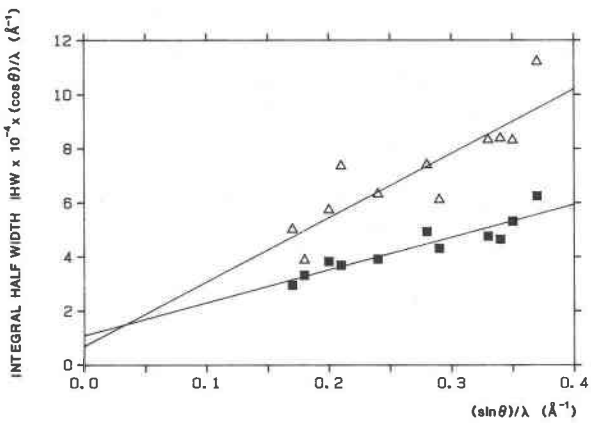

Fig. 1. Physical line broadening of $FeNbO_4$ reflections at 1050°C (△) and 1240°C (■). Slope yields the degree of distortion and the intercept is inversely proportional to the crystallite size.

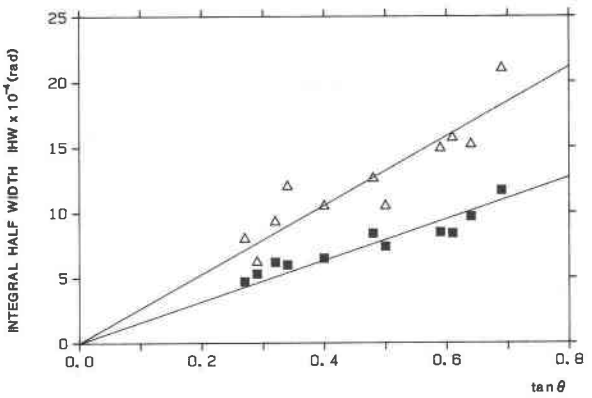

Fig. 2. Line broadening of the $FeNbO_4$ phase, almost entirely dominated by lattice distortions. Distortions decrease with increasing annealing temperature. △: 1050°C, ■: 1240°C.

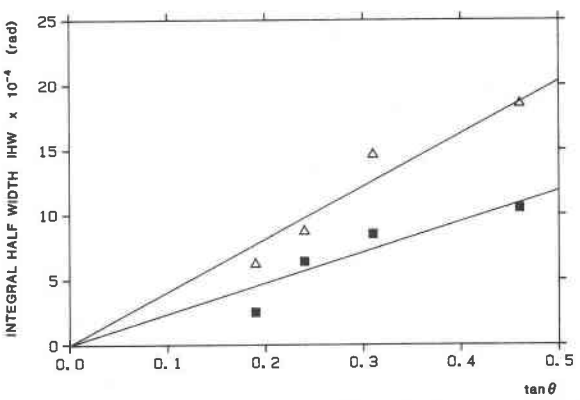

Fig. 3. Line broadening for the $U_3O_8 \cdot 1.5Nb_2O_5$ phase, with only a few lines analyzed. △: 1050°C, ■: 1240°C.

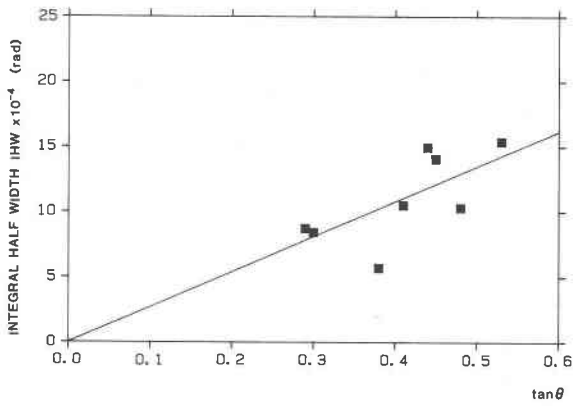

Fig. 4. Line broadening for the $(Y,RE)(Nb,Ta)O_4$ phase at 1240°C. Scattering in the data is partly due to low crystal symmetry (monoclinic).

The data for the $FeNbO_4$ phase are best for estimating cn at different annealing temperatures. The relative difference in the effective atomic volume of the $FeNbO_4$ phase and the amorphous phase can be deduced from the macroscopic densities of 5.36 and 5.7 g/cm^3 respectively. The Poisson ratio is assumed to be 0.35. Using the (202) reflections because they can clearly be recognized even in the 870°C pattern, the following concentrations cn were obtained:

T (°C) :	870	1050	1240
HWB (rad) :	26×10^{-4}	14×10^{-4}	6.2×10^{-4}
cn (vol.%) :	5	3	1

Electron diffraction

The first electron diffraction patterns from metamict minerals were obtained by Christ et al. (1954) on zircon and by Havel (1958) on ampangabeite. In recent years, however, numerous TEM studies of metamict matter have appeared: Sinclair and Ringwood (1981) on zirconolite and perovskite, Ewing and Haaker (1982) on zirconolite, Haaker and Ewing (1979), Headley et al. (1981 a), Yada et al. (1981) and Chan and Buseck (1982) on zircon, Pascucci et al. (1981) on quartz and Headley et al. (1981 b) on numerous metamict materials. This revived interest in the metamict state was stimulated by studies on irradiated solids where processes similar to metamictization were encountered (Hobbs, 1979).

As stated above, no crystalline phases could be found in metamict samarskite powder by the Guinier method, which is one of the most sensitive XRD techniques. Electron diffraction, however, showed that crystalline domains were present in a concentration of <1%. The concentration was estimated when remainders of several independent sedimentation cycles (less than 1 g out of about 50 g in each cycle) were analyzed by X-ray diffraction. The lower limit of phase detection in a powder sample by the Guinier method is about 5 vol.%. Table 3 lists the observed d-spacings obtained by electron diffraction. Although it was not possible to identify the pattern from the JCPDS-file, one could correlate the powder pattern with the SAD pattern. The lengths of the two lattice vectors determined ([110] and [211]) matched the d-values of the two strongest powder lines of 4.44Å and 2.57Å respectively. Reciprocal lattice symmetry in the SAD pattern indicated a f.c.c. type lattice and the powder pattern was indexed accordingly. By indexing the powder pattern it was obvious that diffraction from more than one phase occurred. One might assume the presence of contaminants, such as impurities on the TEM sample grids, those introduced during the particle separation or those resulting from the mineral itself (oxidation in or foreign material in microcracks). So far, the latter two possibilities can be ruled out because several independent sample and specimen preparations were made and all diffraction results were the same. Further, no d-spacing sequence could be attributed to common contaminants found in water (kaolinite, montmorillonite) or in minerals (oxides).

Table 3. Electron powder diffraction data of crystalline domains found in metamict samarskite

I/I_o	d [Å]	(hkl)
100	4.44	(110)
5	3.30	
75 broad	2.57	(211)
5	2.33	
10	2.23	(220)
5	2.08	
5	1.98	(310)
35	1.69	(321)
60	1.49	(411/330)
30	1.28	(422)
30	1.23	(431/510)
5	1.20	
5	1.11	(440)
5	1.02	(611/532)
5	0.97	(541)
5	0.91	
5	0.89	(710)

Most dominant phase indexed only with bcc Bravais lattice and a_o = 6.29 Å

The presence of crystalline regions in metamict minerals has always been an obstacle for a generalized model and explanation of the metamict state. A TEM study by Bursill and McLaren in 1966 concluded that zircon, a widely studied metamict system, consisted of misoriented $ZrSiO_4$ crystallites of about 100Å in size. Very recently, however, Headley et al. (1981) seemed to have found evidence that crystalline regions in metamict zircon were natural alteration products which crystallized later. From this aspect, it cannot be ruled out that the crystalline phases found in metamict samarskite were altered material. Yet it is still puzzling that the phases could not be identified.

Discussion

It has been found that metamict samarskite crystallizes into three crystalline stoichiometric phases when heated to 865°C in air. All three phases show substantial X-ray diffraction line broadening right after crystallization. As temperature increases line broadening decreases and dis-

appears at 1470°C. Line profile analysis suggests that the broadening is caused by nonuniform strains from precipitates of individual phases being compressed by a microcrystalline matrix. In earlier stages of heating below the crystallization temperature nuclei precipitate and stresses become significant due to volume differences. Faessler (1942) reported a density decrease from 5.725 to 5.374 g/cm^3 on metamict and annealed samarskite from Miask (USSR). The volume differences cause compact material to disintegrate into loose powder during heating. On polished surfaces microcracks were observed after heat treatments as low as 400°C. This indicates that nucleation starts well below crystallization temperature. Similar microcracking has been observed on devitrified, ^{244}Cm-doped borosilicate glasses where the cracking has been interpreted as a result of radiation induced swelling of ingrown crystalline phases (Weber et al., 1979). At higher temperatures above crystallization stresses are relaxed and cn, the volume concentration of submicroscopic nuclei which press against growing crystallites of the stable reaction products, decreases. The stress causing nuclei are believed to be the remainder of structurally intermediate precipitates as suggested by Pyatenko (1970) which eventually dissolve at a high enough temperature. Direct evidence of nuclei in the matrix of metamict samarskite has not been found. Crystalline domains were detected by TEM but their concentration is too low to appear characteristic of the metamict state of samarskite.

Natural metamictization has been used as an analogue for long term irradiation effects in synthetic minerals. Zirconolite ($CaZrTi_2O_7$) is one of the main constituents of SYNROC, a ceramic form of nuclear waste, in which active actinides get incorporated (Ringwood et al., 1979). The minerals in SYNROC are subject mainly to alpha-recoil damage resulting from the decay of alpha-emitting radionuclides (Fleischer, 1982). The lattice damage inflicted has been referred to as a metamict state once an X-ray amorphous state has been produced. Heavily damaged, synthetic zirconolite, doped with ^{238}Pu, showed complete amorphization which was characterized as a highly disordered state. Small amounts of crystalline domains were found also and identified as PuO_2 and TiO_2 (Clinard et al., 1981). Natural U and Th bearing zirconolites, on the other hand, were observed to break down into small crystalline domains and eventually reach a X-ray amorphous, but still crystalline state after high enough alpha-doses. No simple oxide phases were detected (Sinclair and Ringwood, 1981). Ewing et al. (1982) attributed crystalline domains observed in natural zirconolites to postmetamict recrystallization and alteration.

On the basis of these somewhat differing results it is difficult to say to what extent irradiation effects in sythetic materials are representative of natural metamictization. In a recent study by Keller and Wagner (1983) it has been found that the structure of metamict samarskite (Mitchell Co.) is truly amorphous rather than microcrystalline. One could speculate that metamict samarskite exhibits a highly defective crystal lattice. X-ray diffraction would again reveal no Bragg-peaks but only atomic short range order maxima. Annealing should restore the lattice damage similar to the annealing of self-irradiated $CmAl_2O_3$ studied by Moseley (1971). When samarskite is annealed crystallization in air is not gradual as it is typical of defective matter (point defects) but occurs within a short time interval at high temperature, depending on the rate of heating and results in three crystalline phases. However, the possibility, that any recovery from radiation damages through annealing remains undetected by the onset of precipitation of phase nuclei, cannot be ruled out.

Summary

It appears that minerals, known as metamict and made metamict, behave differently in the way and to what degree they are susceptible to metamictization. Heat treatment of metamict samarskite in air shows that the premetamict structure was not recovered. Heating of samarskite cannot be considered as an annealing process of radiation induced lattice defects. Rather, heating seems to favor growth of microcrystalline phase nuclei, which cause internal stresses. X-ray profile analysis of stable transformation products from heating indicates that with increasing temperature stress causing nuclei dissolve and stresses are relaxed. The results obtained and a recent study by Keller and Wagner (1983) suggest that the metamict state of samarskite is a glassy state and crystallization by heating is determined by nucleation processes.

Acknowledgments

I wish to thank Drs. W. Klement and C.N.J. Wagner from UCLA for helpful discussions and comments on the manuscript. I am also indebted to Dr. H. Lerz of the Lehrstuhl für Mineralogie, Technische Universität Munich, who made it possible to obtain the sample of samarskite used in this investigation.

References

Berman, J. (1955) Identification of metamict minerals by X-ray diffraction. American Mineralogist, 40, 805–827.

Broegger, W. C. (1893) Amorf: Salmonsens store illustrede Konversationslexikon 1, 742–743. ((abstr.) Über die verschiedenen Gruppen der amorphen Körper. Zeitschrift für Kristallographie, 25, 427–428, 1896)

Bouska, A. (1970) A systematic review of metamict minerals. Acta Universitatis Carolinae-Geologica, 3, 143–169.

Bursill, L. A. and McLaren, A. C. (1966) Transmission electron microscopy study of natural radiation damage in zircon ($ZrSiO_4$). Physica Status Solidi, 13, 331–343.

Cartz, L., Karioris, F. G. and Gowda, K. A. (1981) Metamict states of $ThSiO_4$ dimorphs, huttonite and thorite. Radiation Effects Letters, 67, 83–85.

Chan, I. Y. and Buseck, P. R. (1982) Metamictization in zircon. In G. W. Bailey, Ed., 40th Annual Meeting of the Electron Microscopy Society of America, p. 618–619. Claitor's Publishing Division, Baton Rouge.

Christ, C. L., Dwornik, E. J. and Tischler, M. S. (1954) Crystalline Regions in Metamict Minerals. Science, 119, 513.

Clinard, F. W., Hobbs, L. W., Land, C. C., Peterson, D. E., Rohr, D. L., and Roof, R. B. (1982) Alpha-decay self-irradiation damage in Pu-238-substituted zirconolite. Journal of Nuclear Materials, 105, 248–256.

Evans, H. T., Appleman, D. E., and Handwerker, D. S. (1963) The least square refinement of crystal unit cell with powder diffraction data by an automatic indexing method. (abstr.) Annual Meeting of the American Crystallographic Association, p. 42–43. March 28, Cambridge, Mass.

Ewing, R. C. and Ehlmann, A. J. (1975 a) Annealing study of metamict, orthorhombic, rare earth, AB_2O_6-type, Nb–Ta–Ti oxides. The Canadian Mineralogist, 13, 1–7.

Ewing, R. C. (1975 b) The crystal chemistry of complex niobium and tantalum oxides. IV. The metamict state: Discussion. American Mineralogist, 60, 728–733.

Ewing, R. C. and Haaker, R. F., Headley, T. J., and Hlava, P. F. (1982) Zirconolites from Sri Lanka, South Africa and Brazil. In S. V. Topp, Ed., The Scientific Basis of Nuclear Waste Management, p. 249–256. Elsevier Science Publishing Company.

Faessler, A. (1942) Untersuchungen zum Problem des metamikten Zustandes. Zeitschrift für Kristallographie, 104, 81–113.

Fleischer, R. L. (1982) Alpha-recoil damage and solution effects in minerals: uranium isotopic disequlibrium and radon release. Geochimica et Cosmochimica Acta, 46, 2191–2201.

Graham, J. and Thornber, M. R. (1974) The crystal chemistry of complex niobium and tantalum oxides. IV. The metamict state. American Mineralogist, 59, 1047–1050.

Guinier, A. (1963) X-Ray Diffraction in Crystals, Imperfect Crystals, and Amorphous Bodies. W. H. Freeman and Co., San Francisco.

Haaker, R. F. and Ewing, R. C. (1979) The metamict state radiation damage in crystalline materials. DOE Publication. CONF-790420, 305–309.

Havel, V. (1958) Elektronenbeugung auf metamikten Ampangabeit aus Madagaskar. Die Naturwissenschaften, Heft 9, Jg. 45, 206–207.

Headley, T. J., Ewing, R. C. and Haaker, R. F. (1981 a) High resolution study of the metamict state of zircon. In G. W. Bailey, Ed., 39th Annual Meeting of the Electron Microscopy Society of America, p. 112–113. Claitor's Publishing Division, Baton Rouge.

Headley, T. J., Ewing, R. C., and Haaker, R. F. (1981 b) Amorphous structure of metamict minerals observed by TEM. Nature, 29, 449–450.

Hobbs, L. W. (1979) Application of TEM to radiation damage in ceramics. Journal of the American Ceramic Society, 62, 267–278.

Keller, L. and Wagner, C. N. J. (1983) Diffraction analysis of metamict samarskite. American Mineralogist, 68, 459–465.

Komkov, A. I. (1965 a) Crystal structure and chemical constitution of samarskite. Doklady Akademii Nauk SSSR, 160, 693–696. (Translated Doklady Akademii Nauk SSSR Earth Sciences, 160, 127–129, 1965).

Komkov, A. I. (1965 b) Solid reaction products in the U_3O_8–Nb_2O_5 system. Doklady Akademii Nauk SSSR, 160, 1172–1174. (Translated Doklady Akademii Nauk SSSR Earth Sciences, 160, 129–131, 1965).

Krivoglaz, M. A. (1969) Theory of X-Ray and Thermal Neutron Scattering by Real Crystals. Plenum Press, New York.

Lima De Faria, F. (1964) Identification of Metamict Minerals by X-Ray Powder Photographs. Estudos, Ensaios E Documentos, No. 112.

Mosley, W. C. (1971) Self Radiation Damage in Curium-244 Oxide and Aluminate. Journal of the American Ceramic Society, 54, 475–479.

Pascucci, M. R., Hobbs, L. W. and Hutchinson, J. L. (1981) Lattice image analysis of the metamict transformation in synthetic quartz. In G. W. Bailey, Ed., 39th Annual Meeting of the Electron Microscopy Society of America, p. 110–111. Claitor's Publishing Division, Baton Rouge.

Pyatenko, Y. A. (1970) Behavior of metamict minerals on heating and the general problem of metamictization. Geokhimiya, 9, 1077–1083. (Translated Geochemistry International, 7, 758–763, 1967).

Ringwood, A. E., Kesson, S. E., Ware, N. G., Hibberson, W. O., and Major, A. (1979) The SYNROC process: A geochemical approach to nuclear waste immobilization. Geochemical Journal, 13, 141–165.

Roth, R. S. and Warning, J. L. (1964) Ixiolite and other polymorphic types of $FeNBO_4$. American Mineralogist, 49, 242–246.

Sinclair, W. and Ringwood, A. E. (1981) Alpha-recoil damage in natural zirconolite and perovskite. Geochemical Journal, 15, No. 5, 229–243.

Stokes. A. R. (1948) A Numerical Fourier Analysis Method of The Correction of Widths and Shapes of Lines on X-Ray Powder Photographs. Proceedings of the Physical Society London, 61, 382–391.

Warren, B. E. and Averbach, B. L. (1952) The Separation of Cold Work Distortion and Particle Size Broadening in X-Ray Patterns. Journal of Applied Physics, 23, 497–498.

Weber, W. J., Turcotte, R. P., Bunnell, L. R., Roberts, F. P., and Westsik, Jr. (1979) Radiation effects in vitreous and devitrified simulated waste glass. DOE Publication. CONF-790420, 294–299.

Witt, W. (1964) Zur absoluten Präzisionsbestimmung von Gitterkonstanten mit Elektroneninterferenzen am Beispiel von Thallium-(I)-Chlorid. Zeitschrift für Naturforschung, 19a, 1369–1376.

Yada, K., Tanji, T., and Sunagawa, T. (1981) Application of lattice imaging to radiation damage investigation in natural zircon. Physics and Chemistry of Minerals, 7, 47–52.

Manuscript received, March 8, 1983;
accepted for publication, March 7, 1984.